

# Finite-Size Scaling Study of Aging during Coarsening in Non-Conserved Ising Model: The case of zero temperature quench

Nalina Vadakkayil, Saikat Chakraborty and Subir K. Das

Theoretical Sciences Unit, Jawaharlal Nehru Centre for Advanced Scientific Research, Jakkur P.O., Bangalore 560064, India.

E-mail: das@jncasr.ac.in

June 2018

## Abstract.

Following quenches from random initial configurations to zero temperature, we study aging during evolution of the ferromagnetic (nonconserved) Ising model towards equilibrium, via Monte Carlo simulations of very large systems, in space dimensions  $d = 2$  and  $3$ . Results for the two-time autocorrelations, obtained by using different acceptance probabilities for the spin-flip trial moves, are in agreement with each other. We demonstrate the scaling of this quantity with respect to  $\ell/\ell_w$ , where  $\ell$  and  $\ell_w$  are the average domain sizes at  $t$  and  $t_w$  ( $\leq t$ ), the observation and waiting times, respectively. The scaling functions are shown to be of power-law type for  $\ell/\ell_w \rightarrow \infty$ . The exponents of these power-laws have been estimated via the finite-size scaling analyses and discussed with reference to the available results from non-zero temperatures. While in  $d = 2$  we do not observe any temperature dependence, in the case of  $d = 3$  the outcome for quench to zero temperature is very different from the available results for high temperature and violates a lower bound, which we explain via structural consideration. We also present results on the freezing phenomena that this model exhibits at zero temperature. Furthermore, from simulations of extremely large system, thereby avoiding the freezing effect, it has been confirmed that the growth of average domain size in  $d = 3$ , that remained a puzzle in the literature, follows the Lifshitz-Allen-Cahn law in the asymptotic limit.

*Keywords:* Phase Ordering Dynamics, Aging Phenomena, Ising Model, Monte Carlo, Finite-size Scaling

## 1. Introduction

Following quench from a homogeneous configuration to a state inside the coexistence curve, as a system evolves towards the new equilibrium, various structural quantities exhibit interesting scaling properties [1, 2, 3, 4, 5, 6, 7, 8, 9, 10, 11]. In this context, a rather general order-parameter correlation function is defined by connecting two space points  $(\vec{r}_1, \vec{r}_2)$  and two times  $(t, t_w)$ , and is written as [2]

$$C_{22}(\vec{r}_1, \vec{r}_2; t, t_w) = \langle \psi(\vec{r}_1, t) \psi(\vec{r}_2, t_w) \rangle - \langle \psi(\vec{r}_1, t) \rangle \langle \psi(\vec{r}_2, t_w) \rangle. \quad (1)$$

Here  $\psi$  is a space- and time-dependent order-parameter field. For isotropic structures, which we assume to be true for the cases addressed in this paper, the space dependence in  $C_{22}$  comes through  $r = |\vec{r}_1 - \vec{r}_2|$ , the scalar distance between  $\vec{r}_1$  and  $\vec{r}_2$ . For  $t = t_w$ ,  $C_{22}$ , to be denoted by  $C(r, t)$ , is referred to as the two-point equal-time correlation function [1, 2]. On the other hand, for  $\vec{r}_1 = \vec{r}_2$ , we call  $C_{22}$  the two-time autocorrelation function [2]. The latter quantity, that will be represented by  $C_{\text{ag}}(t, t_w)$ , is often used for studying aging in nonequilibrium systems [2, 3], where  $t_w$  ( $\leq t$ ) is referred to as the waiting time or the age of the system. It is worth mentioning here that  $C_{\text{ag}}(t, t_w)$  may contain information on relaxation related to equilibration inside individual domains as well.

The two-point equal-time correlation function typically exhibits the scaling behavior [1, 2, 9]

$$C(r, t) \equiv \tilde{C}(r/\ell(t)), \quad (2)$$

where  $\tilde{C}$  is a time independent master function [1] and  $\ell$  is the average length of domains that are rich in particles or spins of one or the other type. Usually,  $\ell$  grows in a power-law manner [1], with exponent  $\alpha$ , as

$$\ell \sim t^\alpha. \quad (3)$$

The scaling property in Eq. (2), valid for non-fractal morphology, implies self-similarity, viz., the structures at two different times differ from each other only by a change in the length scale [1]. On the other hand,  $C_{\text{ag}}(t, t_w)$ , in many situations, exhibits the scaling form [2, 3, 4, 6, 7, 8, 11, 12, 13]

$$C_{\text{ag}}(t, t_w) \equiv \tilde{C}_{\text{ag}}(x); \quad x = \frac{\ell}{\ell_w}, \quad (4)$$

where  $\ell_w$  is the characteristic length scale of the system at time  $t_w$ .

There has been serious interest in understanding the forms of these correlation functions for coarsening dynamics with and without conservation [1, 2] of the total value of the order parameter ( $= \int_V d\vec{r} \psi(\vec{r}, t)$ ,  $V$  being the system volume). Remarkable progress has been made with respect to the nonconserved dynamics [1, 2], for scalar as well as vector order parameters. A large fraction of the studies in the nonconserved

variety are related to the coarsening in ferromagnetic Ising model [1, 2] ( $\langle ij \rangle$  stands for nearest neighbors)

$$H = -J \sum_{\langle ij \rangle} S_i S_j, \quad S_i = \pm 1, \quad J > 0, \quad (5)$$

or in the time-dependent Ginzburg-Landau (TDGL) model [1, 2], the latter being essentially a coarse-grained version of the kinetic Ising model.

Ohta, Jasnow and Kawasaki (OJK) [9], via a Gaussian approximation of an auxiliary field [1, 2, 9], obtained an expression for  $C_{22}$  in the case of nonconserved scalar order-parameter. This reads

$$C_{22}(r; t, t_w) = \frac{2}{\pi} \sin^{-1} \gamma, \quad (6)$$

where

$$\gamma = \left( \frac{2\sqrt{tt_w}}{t+t_w} \right)^{d/2} \exp \left[ \frac{-r^2}{4D(t+t_w)} \right], \quad (7)$$

$d$  being the system dimension and  $D$  a diffusion constant. For  $t = t_w$ , from Eqs. (6) and (7) one obtains

$$C(r, t) = \frac{2}{\pi} \sin^{-1} \left[ \exp \left( \frac{-r^2}{8Dt} \right) \right]. \quad (8)$$

On the other hand, for  $r = 0$  and  $t \gg t_w$ , we have

$$C_{\text{ag}}(t, t_w) \sim \left( \frac{t}{t_w} \right)^{-d/4}. \quad (9)$$

Given that [1, 2, 14] the value of  $\alpha$  is 1/2 for the nonconserved Ising model, Eq. (9) implies

$$C_{\text{ag}}(t, t_w) \sim \left( \frac{\ell}{\ell_w} \right)^{-\lambda}; \quad \lambda = \frac{d}{2}. \quad (10)$$

Liu and Mazenko (LM) [4], via somewhat similar Gaussian approximation of the auxiliary field of the order parameter in the TDGL equation, obtained different dimension dependence for  $\lambda$ . Exact solution of the dynamical equation for  $C_{22}$ , that LM constructed, provides the result same as the OJK one in  $d = 1$ . However, (approximate) solutions of the above mentioned equation in  $d = 2$  and 3 provide [4]  $\lambda \simeq 1.29$  and  $\simeq 1.67$ , respectively.

For the exponent  $\lambda$ , Fisher and Huse (FH) [3] provided the bounds

$$\frac{d}{2} \leq \lambda \leq d. \quad (11)$$

Notice here that the lower bound of Eq. (11) coincides with the value quoted in Eq. (10), outcome of the OJK theory. Later, Yeung, Rao and Desai (YRD) [6], by incorporating the structural differences between the conserved and nonconserved dynamics, obtained a more general lower bound as

$$\lambda \geq \frac{d + \beta}{2}, \quad (12)$$

where  $\beta$  is a power-law exponent related to the small wave-number ( $k$ ) enhancement of the structure factor [15, 16]:

$$S(k, t) \sim k^\beta. \quad (13)$$

It has been shown that  $\beta = 0$  for nonconserved Ising dynamics [15, 16]. This leads to the agreement of YRD bound with the FH lower bound. Here note that  $S(k, t)$  is the Fourier transform of  $C(r, t)$  and has the scaling form [1, 2]

$$S(k, t) \equiv \ell^d \tilde{S}(k\ell), \quad (14)$$

where  $\tilde{S}(k\ell)$  is a time independent master function.

Predictions of both OJK and LM follow the FH bounds. We mention here that there exists an argument, related to percolation, by FH [3], that suggests  $\lambda = d - a$ , where  $a$  is the inverse of the exponent for the power-law singularity of the percolation correlation length. This, e.g., provides  $\lambda = 5/4$  in  $d = 2$ . However, FH [3] cautioned about using this argument, as well as their upper bound.

Monte Carlo (MC) simulations of the nonconserved Ising model in  $d = 2$  showed consistency [12, 17] with the OJK function of Eq. (8) and the LM value for  $\lambda$ . The latter fact appeared true [12, 17] in  $d = 3$  as well, for quenches to certain nonzero temperatures ( $T_f$ ) from the initial temperatures ( $T_i$ ) that are far above the critical value ( $T_c$ ). However, the  $d = 3$  Ising model appears to be different and difficult [17, 18, 19, 20, 21, 22, 23, 24, 25] for  $T_f = 0$ . In this case, simulation reports on the time dependence of  $\ell$  differ from the theoretical expectation [14]. While some works reported  $\alpha = 1/3$ , a few reported even slower growth. In recent works [22, 25], it has been shown, via simulations of very large systems, that the (theoretically) expected value  $\alpha = 1/2$  becomes visible only at very late time.

Furthermore, studies with smaller systems, for  $T_f = 0$ , revealed interesting freezing behavior with respect to reaching the expected ground state [23, 24]. Unusual structural aspects were also reported for  $d = 3$  [23, 24]. In the structural context, we showed that  $\tilde{C}$ , unlike the  $d = 2$  case, differs from that at high temperatures [17, 26]. Given the connection between structural and aging properties, discussed above, it is then natural to ask the question: Does there exist difference in the values of  $\lambda$  for  $T_f = 0$  and  $T_f > 0$ ? Our recent letter [26], in fact, suggested the violation of the FH lower bound for  $T_f = 0$  in  $d = 3$ . To confirm that, better analysis of data are needed. Furthermore, even though all the above mentioned studies of kinetic Ising model use (Glauber) spin-flip [27, 28] as trial move during the MC simulations [27], that does not preserve the global order parameter, these moves were accepted with different probabilities in different studies. For example, in our previous studies, Metropolis algorithm [27] was used, whereas Refs. [23] and [24] used the Glauber algorithm [27, 28]. Thus, in addition to providing details related to our recent letter [26] and arriving at appropriate conclusion via more accurate analysis, we also undertake a comprehensive study to compare results from these two different algorithms, including results on the freezing phenomena that prevent the systems from reaching the ground state. Given the anomalies reported at  $T_f = 0$ , this exercise, we feel, is important.

In this paper, all the results are presented from  $T_f = 0$ . Via state-of-the-art finite-size scaling analysis [12, 13, 27, 29, 30, 31, 32] of the MC [27] simulation results, we arrive at the following conclusions for the decay of  $C_{\text{ag}}(t, t_w)$ . We confirm that there exists no temperature dependence in pattern, growth and aging in the case of  $d = 2$ . On the other hand, for  $d = 3$ , the value of the aging exponent, estimated from significantly long period of simulations, indeed violates the FH lower bound. This, however, can be explained via the structural consideration of YRD. On the issue of freezing, in agreement with a previous work, we find that for  $d = 3$  and  $T_f = 0$  systems almost never reach ground state. The frozen length scale, however, is system-size dependent with a linear relationship. Furthermore, for the domain growth, unambiguous confirmation of the  $t^{1/2}$  behavior has been provided. Results obtained by using Metropolis and Glauber algorithms are found to be consistent with each other. Here we state that at  $T_f = 0$  the trial moves that bring no change in the energy are customarily accepted with the probabilities  $p = 0, 1/2$  or  $1$ , the latter two correspond, respectively, to the Glauber and Metropolis methods. For  $p = 0$ , like the previous studies [23, 24], we observe frozen dynamics from very early time and these results are not presented.

The rest of the paper is organized as follows. In Section 2 we discuss the methods. Results are presented in Section 3. Finally we summarize our results in Section 4.

## 2. Methods

Nonconserved coarsening dynamics in the nearest neighbor Ising model, introduced above, for  $T_f = 0$ , is studied via MC simulations [27] in periodic square ( $d = 2$ ) and cubic ( $d = 3$ ) boxes. We have used square lattice in  $d = 2$  and simple cubic lattice in  $d = 3$ . The values of  $T_c$  for this model [27] in  $d = 2$  and  $3$  are respectively  $\simeq 2.269J/k_B$  and  $\simeq 4.51J/k_B$ ,  $k_B$  being the Boltzmann constant.

We have used the Glauber spin-flip moves [28], a standard method to introduce nonconserved dynamics. For a trial move, the sign of a randomly chosen spin is changed. The move is accepted if such a change lowers the energy of the system and rejected if the move increases the energy. For no energy change, one can use different probabilities  $p$  ( $> 0$ ) for accepting the moves [23, 24]. In this work, we have used  $p = 0.5$  and  $1$ , that correspond to Glauber [27, 28] and Metropolis [27] acceptance probabilities, respectively.

Time in our simulations was measured in units of MC steps (MCS) [27], one step consisting of  $L^d$  trial moves,  $L$  being the linear dimension of a system (in units of the lattice constant). For the sake of convenience, in the rest of the paper, we set  $k_B, J$  and the lattice constant to unity.

For the calculation of length [17], we have identified the sizes,  $\ell_d$ , of various domains by scanning a system along different Cartesian directions. Two successive changes in sign in any direction identify a domain and the corresponding distance provides the length, i.e., the value of  $\ell_d$ . The average value,  $\ell(t)$ , was obtained from the first moment

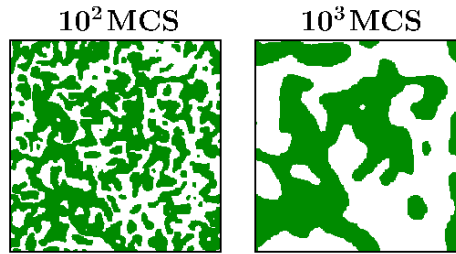


**Figure 1.** Evolution snapshots from the Monte Carlo simulations of the 2D nonconserved Ising model at  $T_f = 0$ , after quenching from  $T_i = \infty$ . These pictures correspond to  $p = 1$ . The marked regions represent “up” spins and the locations of the “down” spins are left unmarked. The linear dimension of the system is  $L = 512$ .

of the time-dependent distributions,  $P(\ell_d, t)$ , thus obtained, i.e.,

$$\ell(t) = \int d\ell_d \ell_d P(\ell_d, t). \quad (15)$$

The value of  $\ell$  can be obtained from the scaling properties [1, 2] of  $C(r, t)$  and  $S(k, t)$  as well [see Eqs. (2) and (14)]. The measures from different functions are expected to provide the same information, apart from different constants of proportionality. Note that the spin variable  $S_i$  is similar to the order parameter field  $\psi$ . Thus, with respect to the calculations of various correlation functions no further discussion becomes necessary.

All our results are presented after averaging over multiple independent initial configurations. This number, for growth and aging, falls in the range between five and 60, depending upon the value of  $L$ . Other than the finite-size effects and freezing phenomena related analyses, all data for the correlation functions are for  $L = 512$ , presented after averaging over 100 and 20 independent initial configurations, in  $d = 2$  and  $d = 3$ , respectively. For the freezing phenomena, given that the studied systems are rather small, we have obtained the quantitative results after averaging over several hundred initial configurations.

### 3. Results

First, we discuss results for  $p = 1$ , in subsection 3.1. Following this, in subsection 3.2 we will present results for  $p = 1/2$ .

#### 3.1. $p = 1$

For the sake of completeness, as well as for the convenience of later discussion, we start by presenting results for the pattern and growth. In Fig. 1 we show snapshots taken during the evolution of the nonconserved Ising model at  $T_f = 0$ . These snapshots are from MC simulations in  $d = 2$ . Growth in the system is clearly visible. To check for the self-similarity, in Fig. 2 we show scaling plots of the two-point equal-time correlation function. In this figure, we present data from both  $d = 2$  and 3. Nice collapse of data, in both the dimensions, from different times, when plotted versus  $r/\ell$ , confirms self-similar

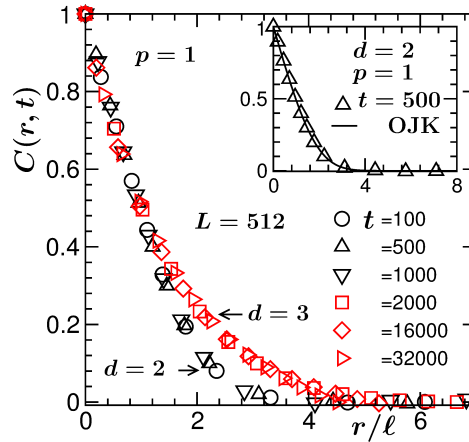


**Figure 2.** Scaling plots of the two-point equal-time correlation function. We have shown  $C(r, t)$  as a function of  $r/l$ , for both  $d = 2$  and  $3$ . In each dimension data from three different times are included. The used values of  $l$  in this figure were obtained from  $C(l, t) = 0.5$ . For all the other purposes we have used  $l$  obtained from the first moment of the domain size distribution function  $P(l_d, t)$ . Inset: Plot of  $C(r, t)$  versus  $r/l$  for  $d = 2$  and  $t = 500$ . The continuous curve there is the Ohta-Jasnow-Kawasaki function. All results are for  $p = 1$ .

character [1, 2] of the growth. Interestingly, the master curves from  $d = 2$  and  $d = 3$  do not match with each other [17]. As shown in the inset, the  $d = 2$  data are in agreement with the OJK function [9, 17]. We note here,  $C(r, t)$  at high temperatures, for both the dimensions, agree well with the OJK form [17]. This states the fact that the pattern at  $T_f = 0$ , in  $d = 3$ , is special. This is in line with previous reports by other authors [17, 18, 19, 20, 21, 22, 23, 24, 25, 26] and will be useful in explaining new observation with respect to aging property.

In Fig. 3 we present data for domain growth, viz., we show  $l(t)$  versus  $t$ , on a log-log scale. Results from both the dimensions are included. The 2D data exhibit a unique power-law behavior, with  $\alpha \simeq 1/2$ , over an extended period of time. The departure from the above scaling in the long time limit, clearly seen for  $L = 512$  (shown with symbols), is due to finite-size effects. While this behavior in  $d = 2$  is same as the results from nonzero temperature, the case of  $d = 3$  is very different from our observation for coarsening at  $T_f$  higher than the roughening transition [33] (here note that in  $d = 2$  there does not exist a nonzero roughening transition). The 3D data in Fig. 3, after a brief initial period (with higher exponent corresponding to annihilation of local defects), displays [7, 17, 18, 19, 20, 21] growth with  $\alpha \simeq 1/3$  over more than two decades in time. At very late time the data exhibit a crossover [17, 22, 25] to  $\alpha \simeq 1/2$ . Towards the end of the presented time window, we see signature of finite-size effects for  $L = 512$  (see the data set with symbols).

With respect to the appearance of finite-size effects, however, there is similarity between the 2D and 3D cases. See the deviation of data with symbols, corresponding to  $L = 512$  for both the dimensions, at  $l \simeq 205 (= 0.4L)$ , marked by the dashed horizontal

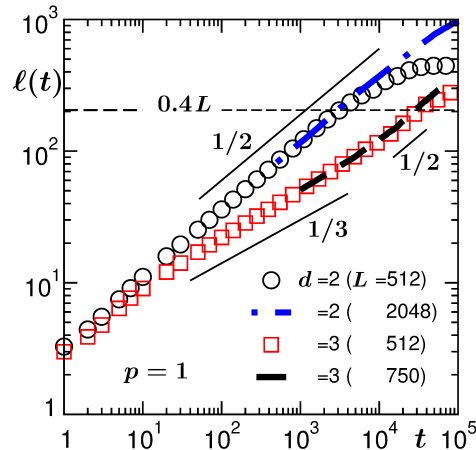


**Figure 3.** Log-log plots of average domain size versus time, for  $p = 1$ . We have shown data from both the dimensions. The continuous lines represent various power laws, exponents for which are mentioned in the figure. The dashed horizontal line, at  $\ell = 0.4L$ , marks the appearance of finite-size effects for data sets corresponding to  $L = 512$ .

line. For larger system size (see the dashed line for  $d = 3$  with  $L = 750$  and the dashed-dotted line for  $d = 2$  with  $L = 2048$ ), of course, the growth with  $\alpha = 1/2$  is more prominent due to lesser effects of finite system size over the presented time range. Note that such a clear confirmation of  $t^{1/2}$  behavior for extended period of time in  $d = 3$  could not have been previously possible because of consideration of much smaller system sizes. The appearance of finite-size effects at  $\ell \simeq 0.4L$  at  $T_f = 0$  is very similar to that for non-zero values of  $T_f$ . We mention here, in the 3D case the very late time finite-size behavior for  $T_f = 0$  is rather complex [23, 24]. The systems almost never reach the ground state (this problem is perhaps less severe in  $d = 2$ ) even at the end of extremely long simulation runs [23, 24, 34, 35]. One may anticipate this fact to be somewhat more severe for  $p < 1$ , which we will investigate later. Now we move to the aging property, the primary objective of the work.

In Figs. 4(a) and 4(b) we demonstrate the scaling property of the autocorrelation function [17]. In these figures, we have plotted  $C_{\text{ag}}(t, t_w)$  versus  $\ell/\ell_w$ , for different values of  $t_w$ . Results in Fig. 4(a) are from  $d = 2$ , whereas the  $d = 3$  data are presented in Fig. 4(b). Very nice collapse of data can be appreciated for both the dimensions. Deviations from the collapse, for large values of the abscissa variable, are related to finite-size effects [12, 13]. This occurs at a smaller value of  $x$  for a larger choice of  $t_w$ , as expected. This is because, for a higher value of  $t_w$  smaller fraction of the system size is available for further growth. For  $d = 3$ , the presented data did not suffer as much from the finite-size effects. In this dimension running simulations for large systems over very long period, to observe such effects, is computationally very demanding. Note that the appearance of finite-size effects in the autocorrelation function again complies with our above quoted limit  $\ell \simeq 0.4L$  that we observe for the domain growth. The solid lines in these figures are power-laws with LM values of  $\lambda$ . Clearly, there exist discrepancies between the LM



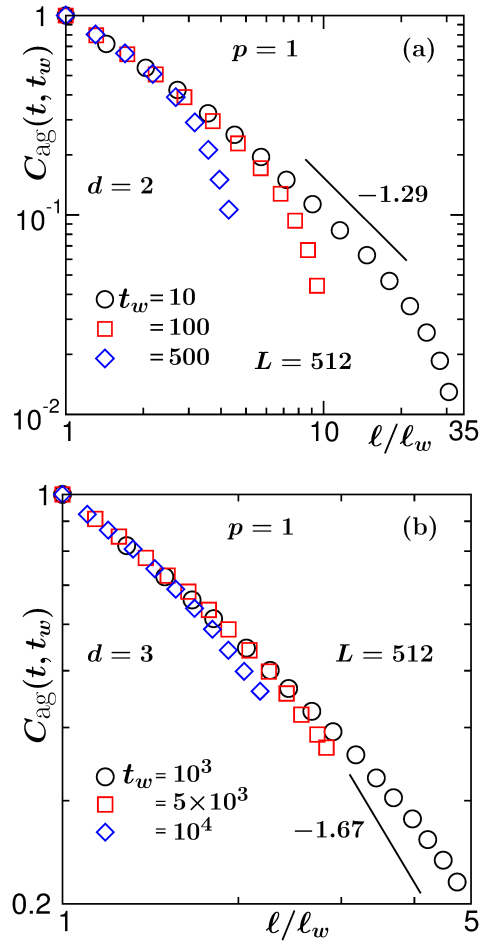


**Figure 4.** (a) Log-log plots of the autocorrelation function,  $C_{\text{ag}}(t, t_w)$ , vs  $\ell/\ell_w$ , for  $d = 2$ . Results from a few different values of  $t_w$  are shown. The solid line corresponds to a power-law decay with exponent  $\lambda = 1.29$ . (b) Same as (a), but here the results are from  $d = 3$ . The solid line here has the power-law exponent  $\lambda = 1.67$ . All the results correspond to  $p = 1$ .

exponents and the simulation results. Furthermore, we observe continuous bending [12] in the scaling functions obtained from the simulations, on the log-log scale. This, of course, is possible when there exist corrections to the power-law scaling [12]. In such a situation, calculation of the instantaneous exponent [4, 12, 13, 36, 37],

$$\lambda_i = -\frac{d \ln C_{\text{ag}}}{d \ln x}, \quad (16)$$

can provide useful information.

In Fig. 5(a) we show  $\lambda_i$ , as a function of  $1/x$  (recall,  $x = \ell/\ell_w$ ), for the  $d = 2$  case. Results for two different system sizes, for a fixed value of  $t_w$ , are included. Corresponding  $C_{\text{ag}}(t, t_w)$  versus  $x$  plots, on log-log scale, are shown in the inset. Data for the smaller value of  $L$  deviate from a linear behavior, as  $x$  increases, when the value of  $x$  is approximately 2. This is due to the finite-size effects and can be appreciated from the continued linear trend, up to much larger value of  $x$ , exhibited by the data

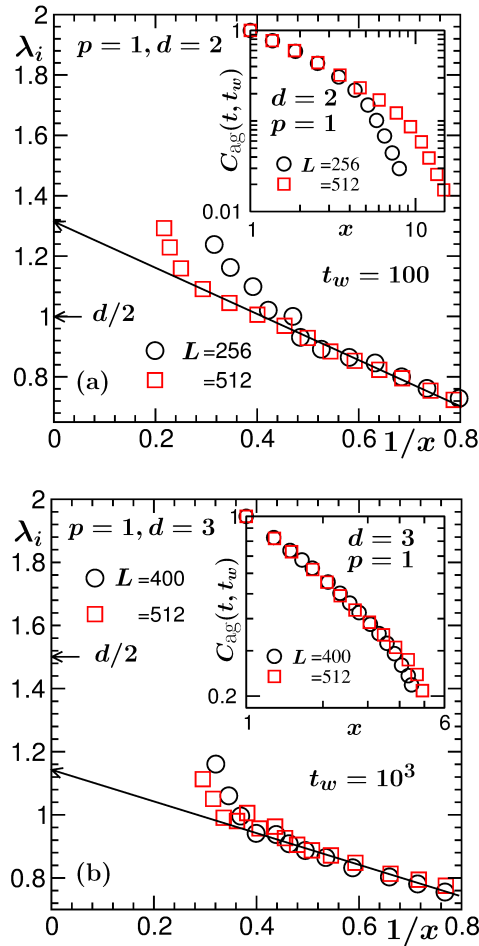


**Figure 5.** (a) Instantaneous exponent,  $\lambda_i$ , for the  $d = 2$  Ising model, is plotted as a function of  $\ell_w/\ell$ , for different system sizes. The value of  $t_w$  is mentioned on the figure. The solid line is a guide to the eye. (b) Same as (a), but the results here are from  $d = 3$ . In both the figures the FH lower bounds have been marked by  $d/2$ . The insets in (a) and (b) show corresponding results for  $C_{\text{ag}}(t, t_w)$  versus  $\ell/\ell_w$ , on log-log scale. All the results were obtained by fixing  $p$  to 1.

from the larger value of  $L$ . Results for different values of  $t_w$ , for fixed  $L$ , provide similar information. This is, as stated above, because of lesser effective system size available for larger  $t_w$ .

A linear extrapolation to  $x = \infty$ , using data unaffected by finite-size effects, provides a value of  $\lambda$  close to 1.3. Invoking the linear behavior,

$$\lambda_i = \lambda - B/x, \quad (17)$$

in the definition in Eq. (16), one obtains an exponential correction factor [12, 13], i.e.,

$$C_{\text{ag}}(t, t_w) = Ae^{-B/x} x^{-\lambda}, \quad (18)$$

$A$  and  $B$  being constants. This implies, a power law can be realized only in the  $t \gg t_w$  limit. Like in the critical phenomena here also it is natural to expect that the corrections should be described by power-laws. However, separately estimating

exponents for corrections of different orders is a difficult task. Given the trend of the data sets, the exponential factor appears to describe the corrections reasonably well. We will make further comment on the accuracy of this full form later.

Similar linear behavior is observable in Fig. 5(b) where we have presented data for  $d = 3$  (again, for corresponding  $C_{\text{ag}}(t, t_w)$  versus  $\ell/\ell_w$  plots see the inset). In this case, the data exhibit convergence to a value [26] between 1.1 and 1.2. While for  $d = 2$  the convergence is consistent with that for higher temperature [12], there exists serious departure in the case of  $d = 3$  from the LM prediction. Note that the LM prediction in  $d = 3$  matches well with the conclusions from the simulation studies at higher temperatures, above the roughening transition [12]. Furthermore,  $\lambda \simeq 1.15$  is far below the lower bound of FH.

Even though reasonably accurate estimate is possible from such extrapolations, one can do better by performing finite-size scaling analysis [12, 13], given that the data for  $\lambda_i$ , at large  $x$ , may suffer from statistical error and finite-size effects, preventing unambiguous choice of regions for performing a linear fit. A finite-size data collapse exercise will be further useful for bringing confidence in the form of Eq. (18), which essentially is an empirical form.

In a finite-size scaling method one looks for collapse of data from various system sizes [27, 29, 30]. Such a method for the analysis of the data for autocorrelation function was recently constructed [12, 13]. See Refs. [38] for more recent work with a different system. Like in the critical phenomena [27, 29, 30], here also one introduces a scaling function  $Y$ . To make  $Y$  independent of system size, we search for a dimensionless scaling variable  $y$ . Since  $x (= \ell/\ell_w)$  is already dimensionless, we choose  $y = x'/x$ , where  $x' = L/\ell_w$ . This provides

$$y = \frac{L}{\ell}. \quad (19)$$

For the sake of convenience, we intend to write  $C_{\text{ag}}(t, t_w)$  as a function of  $y$ . Then,

$$C_{\text{ag}}(t, t_w) = Ae^{-By/y_w} \left( \frac{y_w}{y} \right)^{-\lambda}, \quad (20)$$

where  $y_w = L/\ell_w$ , i.e., the value of  $y$  at  $t = t_w$ . Next, we write the finite-size scaling function, a bridge between thermodynamic and finite-size limit behavior, as

$$Y = C_{\text{ag}}(t, t_w)e^{By/y_w}y_w^\lambda. \quad (21)$$

In the above equation we have absorbed  $y^\lambda$  inside  $Y$ .

We stress again that the choice of  $x'$  above is driven by the dimension of  $x$  and the fraction of the total system size available to explore, given that the measurement starts at  $t_w$ . Coming back to the above comment “fraction of the total system size available to explore”, we mention that this quoted fact allows a finite-size scaling analysis only via the variation of  $t_w$ , without exploring different system sizes. This is because, we state again, with the variation of  $t_w$ , the above mentioned fraction varies, providing different effective system sizes. This fact we will demonstrate by achieving collapse of data from different values of  $L$  and  $t_w$ .

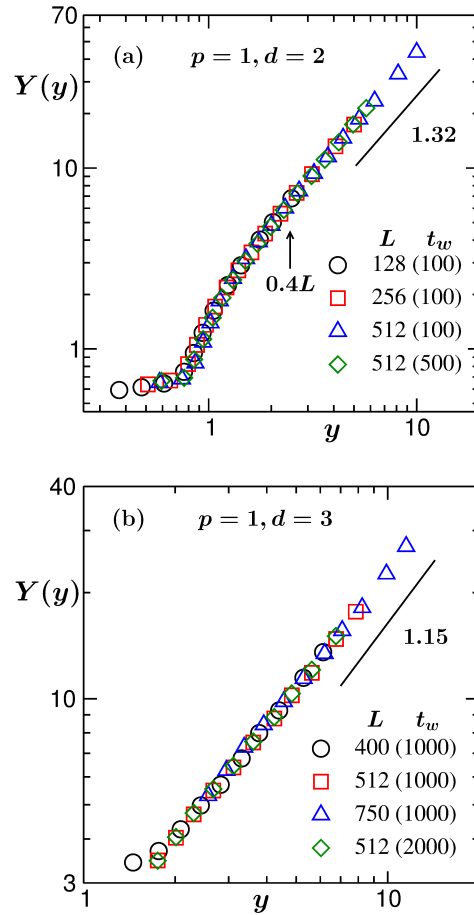


**Figure 6.** (a) Finite-size scaling analysis of the autocorrelation function in  $d = 2$ . The vertical arrow marks the departure of the scaling function from the  $y^\lambda$  behavior. (b) Same as (a), but here it is for  $d = 3$ . The solid lines represent power-laws with the values of exponent mentioned next to them. All results are for  $p = 1$ .

The limiting behavior of  $Y$  can be described as follows. In the thermodynamic limit, i.e., for  $\ell \ll L$  ( $y \rightarrow \infty$ ), we can write

$$Y = Ay^\lambda, \quad (22)$$

so that Eq. (20) is recovered. In the other limit, in finite systems, particularly due to frozen dynamics, we do not expect  $C_{\text{ag}}(t, t_w)$  to vanish. This may lead to a rather flat appearance of  $Y$  for small  $y$ . Such characteristic features, along with a collapse of data from various different  $L$  and  $t_w$  values, can be realized if  $\lambda$  is chosen appropriately, alongside the constant  $B$ . In our data collapse exercise we will treat these two quantities as adjustable parameters.

At nonzero temperatures, there exists coupling between equilibration of domain magnetization and that of the whole system [2], till large value of  $x$ . Given that the former is related to the critical fluctuation [39], for very low value of  $T_f$ , the relaxation related to the domain magnetization occurs very fast, to a value almost unity. Nevertheless, a minor jump in the autocorrelation function very close to  $x = 1$ ,

providing a higher effective exponent for very small  $x$ , exists. Thus, we avoid the data point corresponding to  $x = 1$  in all cases, for the finite-size scaling analysis. Furthermore, scaling of  $C_{\text{ag}}$ , with respect to  $\ell/\ell_w$ , is expected to be observed from rather small values of  $t_w$ , very small  $T_f$ . Nevertheless, deviations at early time is observed, particularly in  $d = 3$ . This may be due to slow crossover to  $t^{1/2}$  growth behavior extending up to very late time. Thus, for this scaling analysis, we have chosen rather large values of  $t_w$  in this dimension.

Even though in an earlier study [12] (for high temperatures) we have obtained good data collapse by using finite-size  $\ell$  in the scaling variable  $y$ , ideally one should use the thermodynamic limit values. There can be two possible ways: (i) to adopt  $\ell \sim t^{1/2}$  behavior, (ii) to use length from a much larger system size that does not exhibit finite-size effects over the time-scale of analysis. We follow the latter method here (as well as for  $p = 1/2$ ) – for  $d = 2$ ,  $\ell$  will be taken from  $L = 2048$  and for  $d = 3$ , we will use  $\ell$  from  $L = 750$ .

Results from the finite-size scaling analysis for  $d = 2$  are presented in Fig. 6 (a), whereas corresponding results for  $d = 3$  are presented in Fig. 6 (b). In the case of  $d = 2$ , very good collapse of data, along with consistency with the limiting behavior discussed above, is obtained for  $\lambda = 1.32$  and  $B = 0.80$ . This value of  $\lambda$ , within statistical error, is in agreement with a previous study [12] for  $T_f = 0.6T_c$  and consistent with the prediction of LM. In the large  $y$  limit the data are consistent with the power-law amplitude  $A \simeq 2$ . This can be appreciated by considering  $C_{\text{ag}}(t, t_w) = 1$  at  $x = 1$  and  $B = 0.8$ . The departure from the power-law behavior is marked by a vertical arrow in Fig. 6 (a). This corresponds to  $\ell = 0.4L$  where finite-size effects occur. A robust power law behavior for  $Y$  till the finite-size effects appear, irrespective of the system size, provide confidence in the exponential correction factor. In this connection, also note that for  $L = 512$  and  $t_w = 100$ , the power-law behavior extends over  $t - t_w$  ranging between 0 and approximately 3600. One may think of improving accuracy in the estimation of  $\lambda$  by allowing for an adjustable exponent in Eq. (17), by replacing  $x$  by  $x^\gamma$ . This exponent will, of course, appear in the argument of the exponential factor. We caution here that the scaling analysis will be less reliable if  $\gamma$  is included, due to large number of adjustable parameters. The information with respect to the departure point of the scaling function from the power-law is quantitatively similar in other cases as well. So, we will not discuss it again.

For  $d = 3$ , on the other hand, the number for the exponent  $\lambda$  turns out to be 1.15, which is very different from that at  $0.6T_c$  [12]. Again note that the high temperature result in this dimension is in good agreement with the LM value. Furthermore, the value of  $\lambda$  at  $T_f = 0$  is far below the lower bound of FH and this conclusion is consistent with that from the analysis of the instantaneous exponent. The question then comes, is it a true violation of the bound? This can perhaps be understood from the derivation of YRD. Before moving to that discussion we briefly point out the intermediate range features of  $Y$  in Fig. 6. Before exhibiting a nearly flat behavior the 2D data fall rather sharply, compared to the 3D case. This may be related to the more prominent freezing

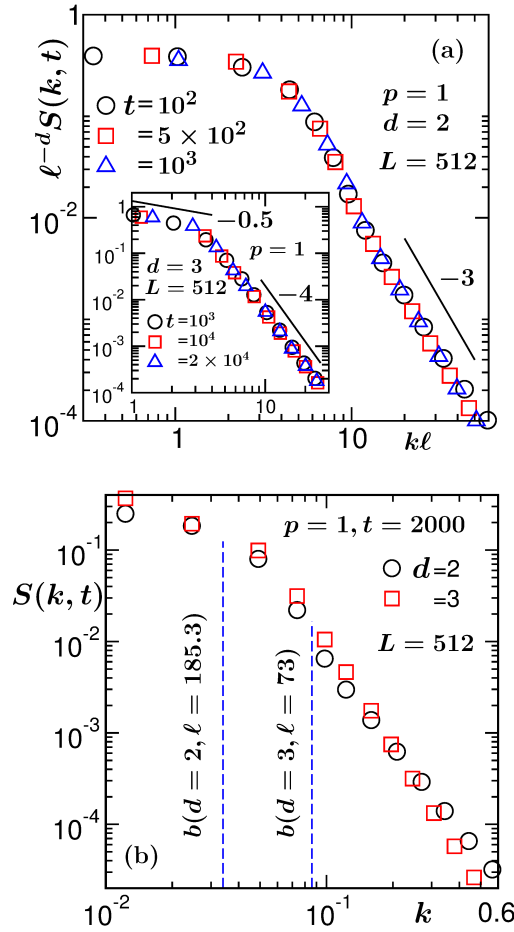


**Figure 7.** (a) Scaling plots of the structure factor in  $d = 2$  (main frame) and  $d = 3$  (inset). The solid lines are power-laws, exponents for which are mentioned in the figure. (b) Plots of the structure factor, vs  $k$ , on a double-log scale, for  $d = 2$  and  $d = 3$ . The dashed vertical lines are explained in the text. These results are for  $p = 1$ .

phenomena in the latter dimension. This fact, as promised, we will discuss later.

In Fig. 7(a) we show the plots of  $S(k, t)$  from  $d = 2$  (main frame) and  $d = 3$  (inset). Our focus here is to obtain the scaling behavior of Eq. (14). Nice collapse of data, in both the dimensions, signify that the chosen values of  $t_w$  for the finite-size scaling analyses are well inside the scaling regime of structure and growth. The power-laws with exponent  $-3$  and  $-4$  represent the Porod law [40, 41] in  $d = 2$  and  $3$ , respectively.

Using the equal time structure factors at  $t_w$  and  $t$ , YRD arrived at

$$C_{\text{ag}} \leq \ell^{d/2} \int_0^b dk k^{d-1} [S(k, t_w) \tilde{S}(k\ell)]^{1/2}, \quad (23)$$

in which they substituted the small  $k$  behavior of  $S(k, t_w)$  [cf. Eq. (13)], to obtain the lower bound. In Eq. (23),  $b$ , the upper limit of the integration, equals  $2\pi/\ell$ . In Fig. 7(b) we present  $S(k, t)$  vs  $k$  plots on a log-log scale from  $d = 2$  and  $3$ . For both the dimensions we have chosen  $t = 2000$  MCS. The vertical dashed lines there correspond to the upper limit  $b$  for different dimensions, corresponding to a time ( $10^4$

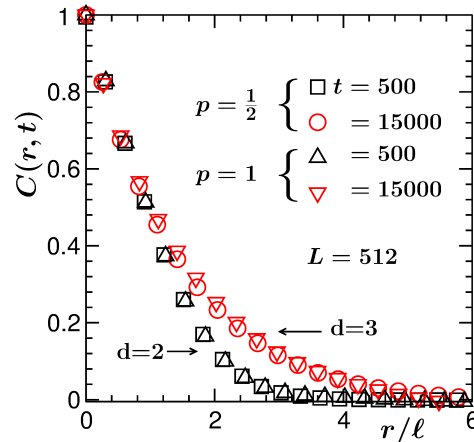


**Figure 8.** Two-point equal-time correlation functions, from MC simulations of the nonconserved Ising model in  $d = 2$  and  $3$ , obtained by using  $p = 1/2$  and  $1$ , are compared. The distance axis is scaled by the average domain length  $\ell$ . Like in Fig. 2, here also the value of  $\ell$  was obtained as the distance at which  $C(r, t)$  decays to half its maximum value.

MCS) reasonably larger than 2000 MCS. It appears, the upper limit of integration for  $d = 3$  covers a significant range of  $k$  over which  $S(k, t)$  decreases, providing an “effective” negative value of  $\beta$ . Given that the growth of  $\ell$  is much slower in  $d = 3$  than in  $d = 2$  over a long intermediate period, one needs to go to very long time to access  $\beta = 0$  behavior. Even then, notice that a negative value of  $\beta$  can already be appreciated from small  $k$  regime in the inset of Fig. 7(a). Thus, even if a crossover occurs to the value predicted by LM, simulations with much larger systems with orders of magnitude longer period of time will be needed to observe that. For that purpose, a change in pattern may also be necessary at such late time.

As stated earlier, an objective of the paper is to compare MC simulation results with different algorithms, viz., we intend to check if there are any differences in the outcomes when trial moves bringing no energy change are accepted with probabilities [23, 24, 27]  $p = 1$  and  $1/2$ . Having presented the results for  $p = 1$ , next we focus our attention to the case with  $p = 1/2$ , with occasional direct comparison of the results with those for  $p = 1$ , wherever seem important.

### 3.2. $p = 1/2$

In Fig. 8 we present comparative results for the two-point equal-time correlation function. This figure contains data from both the dimensions, for  $p = 1/2$  as well as for  $p = 1$ . It appears that the results for  $p = 1/2$  nicely overlap with those for  $p = 1$  when the distance axis is appropriately scaled by the corresponding average domain sizes. These results confirm that both the algorithms provide similar structure.

Fig. 9 (a) shows log-log plots of  $\ell$  versus  $t$ , for both the dimensions. Here we have included data only from the  $p = 1/2$  case. Like in the  $p = 1$  case, the 2D data appear consistent with the theoretical expectation all the way till the finite-size effects appear

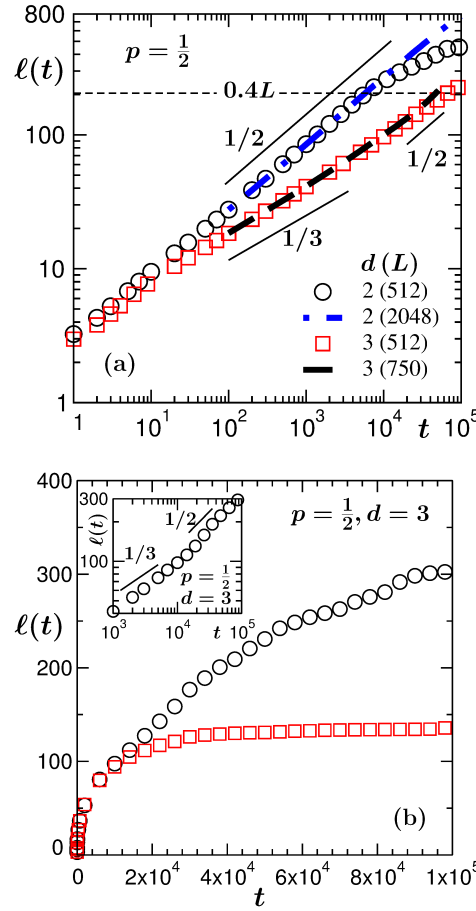


**Figure 9.** (a) Log-log plot of average domain length versus time. We have shown data from  $d = 2$  and  $3$ . The continuous lines represent power-laws, exponents being mentioned next to them. The dashed horizontal line marks the appearance of finite-size effects, at  $\ell = 0.4L$ , for  $L = 512$ . (b) Plot of domain length versus time in  $d = 3$ , for two different initial configurations. Inset shows a log-log plot of average domain size versus time for the data set that did not undergo freezing. These results are obtained with  $p = 1/2$ .

[17] at  $\ell \simeq 0.4L$ . For  $L = 512$ , see the departure of the data set from that of  $L = 2048$ . Plot for the  $d = 3$  case also exhibits a trend similar to the  $p = 1$  case – there exists a consistency of the data set with an exponent  $\alpha \simeq 1/3$  for nearly three decades in time, after which a crossover appears. This is very clearly visible in the  $L = 750$  case. By examining the  $L = 512$  data one may conclude that the finite-size effects appear a little earlier than when  $\ell$  reaches  $0.4L$ . This could well be due to statistical reasons. Here note that runs for many initial configurations get trapped in metastable states very early, without allowing us to appropriately probe the post-crossover region. Data presented in Fig. 9 (a) are averaged by including such runs as well. In Fig. 9 (b) we show  $\ell$  versus  $t$  data for two typical runs, on linear scale. It is clear that some runs can encounter freezing around the time (or even before) when a crossover is expected. This necessitates either extremely good statistics or very large system size. In the inset of this figure, we



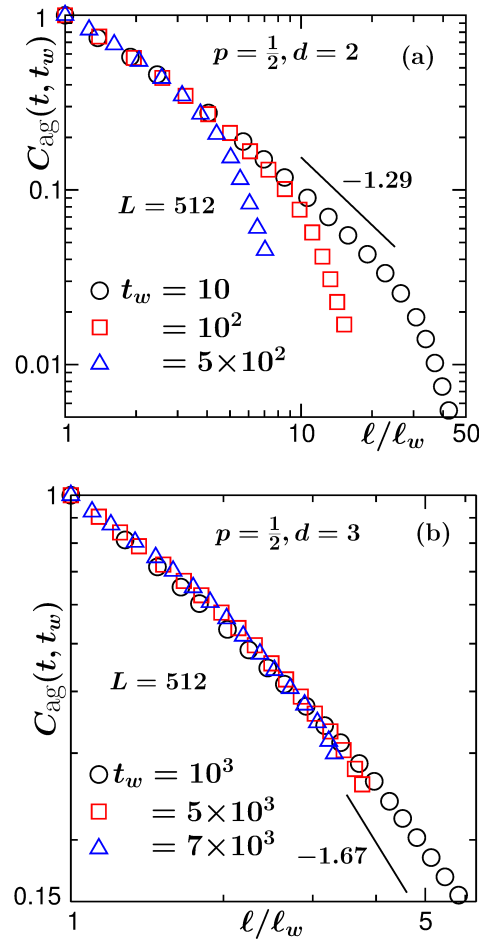


**Figure 10.** (a) Two-time autocorrelation functions, from  $d = 2$ , for different values of  $t_w$ , are plotted versus  $l/l_w$ , on a log-log scale. (b) Same as (a) but for  $d = 3$ . The solid lines represent power-laws, exponents for which are mentioned in the figures. All results correspond to  $p = 1/2$ .

show the plot for the data set that did not show a signature of freezing, on a log-log scale. Clearly, a  $t^{1/2}$  behavior is very prominent towards the end. This overall picture is true for both values of  $p$ . We will provide further discussion on freezing phenomena towards the end of this subsection. Next we present results for aging.

Figs. 10 (a) and 10 (b) are similar to that of Figs. 4 (a) and 4 (b), except for the fact that here we present autocorrelation function for  $p = 1/2$ . Nice collapse of data from different  $t_w$  values are visible when plotted versus  $l/l_w$ . The runs for  $d = 3$  [Fig. 10 (b)] are not long enough to see the finite-size effects as clearly as in the  $d = 2$  case [Fig. 10 (a)]. Once again, even though there exist bending in the log-log plot, data in both the dimensions appear to get linear at late time, implying power-law decay with correction for finite  $x$ . While the 2D results appear reasonably consistent with the LM exponent, strong discrepancy can be seen in the case of  $d = 3$  (see comparison of the simulation data with the solid lines). These facts are consistent with our observation for  $p = 1$ .

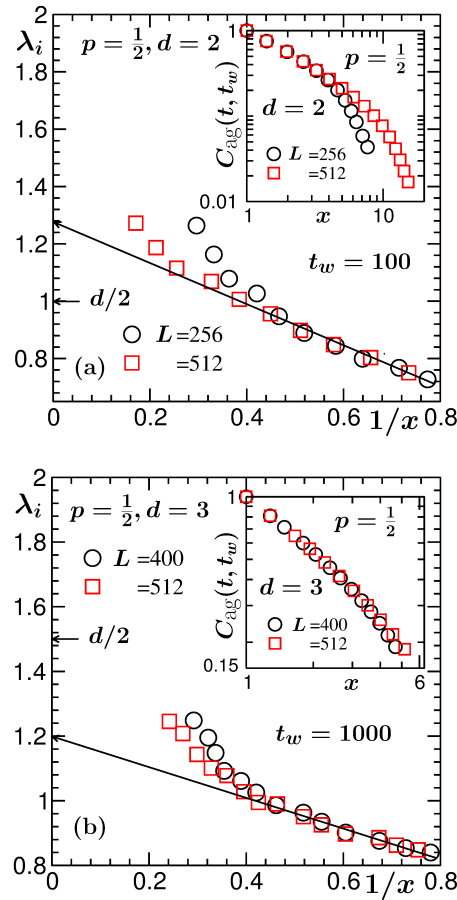


**Figure 11.** Plots of instantaneous exponent  $\lambda_i$  versus  $1/x$  ( $x = \ell/\ell_w$ ), from (a)  $d = 2$  and (b) 3. We have fixed the value of  $t_w$ , and in each dimension, presented results from two different system sizes. The solid straight lines are guides to the eye. The FH lower bounds have been marked by  $d/2$  in both (a) and (b). Corresponding direct plots, i.e., data for  $C_{ag}(t, t_w)$  versus  $x (= \ell/\ell_w)$ , are shown in the insets. These results are from simulations with  $p = 1/2$ .

To quantify the power-law exponents in the asymptotic limit, we calculate the instantaneous exponent [12, 13, 37]  $\lambda_i$ . The corresponding results for  $d = 2$  and 3, vs  $1/x$ , are plotted in Figs. 11 (a) and 11 (b), respectively (see the corresponding  $C_{ag}(t, t_w)$  versus  $\ell/\ell_w$  plots in the insets), for different system sizes. The finite-size behavior appear consistent with the previous subsection. Furthermore, the data sets show convergence to values that are also consistent with the  $p = 1$  case (for comparison see Fig. 5). This is further confirmed by the finite-size scaling analysis plots which are presented in Fig. 12 [see (a) for  $d = 2$  and (b) for  $d = 3$ ]. This exercise, as stressed earlier, discards any possibility of large errors that may appear due to finite size, statistical fluctuation or freezing effects. From the analysis we quote  $\lambda \simeq 1.32$  in  $d = 2$  and  $\lambda \simeq 1.2$  in  $d = 3$ . Given that the two-point equal-time correlation functions from the two algorithms match nicely (see Fig. 8) with each other, viz, for  $p = 1/2$  and  $p = 1$ , we do not take the route of explaining the violation of the FH bound in  $d = 3$  via the

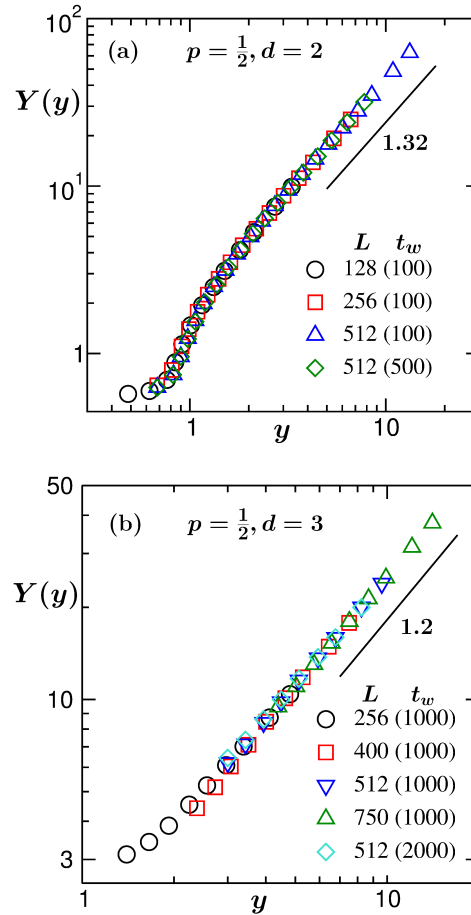


**Figure 12.** (a) Finite-size scaling analysis of the autocorrelation function in  $d = 2$ . (b) Same as (a) but for  $d = 3$ . Both the plots are for  $p = 1/2$ . The solid lines represent power-laws with exponents  $\lambda = 1.32$  and  $\lambda = 1.2$  in  $d = 2$  and  $3$ , respectively.

structure factor again. Rather, below we focus on the issue of freezing.

The reason for discussing freezing is the following. Typically, in many real physical situations, the final (frozen) length scale,  $\ell_f$ , does not depend upon the system size [42, 43, 44, 45]. In many systems the value of  $\ell_f$  is set by a distance related to the repulsive barrier in the interacting potential [42, 43, 44]. Such a picture related to barrier, however, is not expected in the current situation. Nevertheless, to rule out that none of the presented results are affected by this freezing phenomena, we need to know if there exists any system-size dependence of  $\ell_f$ .

In Fig. 13 (a) we show final configurations from two different initial random compositions in  $d = 2$ . The one on the left corresponds to the ground state and the other represents a frozen state. In Fig. 13 (b) we show a frozen configuration from  $d = 3$ . For both  $d = 2$  and  $3$ , the presented configurations are obtained by using  $p = 1/2$ . As opposed to the right frame in  $d = 2$ , where it is easily identifiable that no further growth can occur,  $d = 3$  structure is more complex. Details on this can be found in Refs. [23, 24, 26, 46].

We observe that for a particular system size, for different initial configurations,  $\ell_f$  varies significantly in  $d = 3$ , almost never reaching  $L$  [23, 24]. Whereas in  $d = 2$ , the frozen states are related to the stripe structure seen in Fig. 13 (a). Distributions of  $\ell_f$ ,  $P(\ell_f)$ , for both  $p = 1/2$  and 1, obtained from such variation, are shown in Fig. 14 (a), for  $d = 2$ ,  $L = 200$ ; and in Fig. 14 (b), for  $d = 3$ ,  $L = 70$ . The average values,  $\langle \ell_f \rangle$ , that can be extracted from these distributions turn out to be approximately same for  $p = 1$  and  $p = 1/2$ . The observation is similar for other values of  $L$ . In the case of  $d = 3$  we observe a single peak, with reasonably large width, whereas there exist two spikes in  $d = 2$ . These spikes are related to the ground and stripe states (we have ignored the diagonal stripes). From the height of the two peaks, it can be appreciated that the ground state is reached approximately twice as often as the stripe states [46]. This fact also states that freezing is a more severe problem in  $d = 3$  than in  $d = 2$ .

In Fig. 14 (c) and 14(d) we plot  $\langle \ell_f \rangle$  as a function of  $L$ , for  $p = 1/2$ , in  $d = 2$  and 3, respectively. The dependence in both the dimensions turns out to be linear. Here it is worth mentioning that occasionally artificial freezing in computer simulations can be observed, for slow dynamics, due to periodicity in random numbers, when system sizes are very large. To us, this also does not appear to be true in the present case. Here the phenomena can be attributed to the structure. How the system size at this temperature is affecting the structure and dynamics, to provide a linear relation between frozen length and system size, is an intriguing question. The observation, nevertheless, provides confidence, by looking at the numbers in the plots [Figs. 14(c) and 14 (d)], that our presented results on growth and aging did not suffer from this effect. Here we recall that finite-size effects start appearing when  $\ell \simeq 0.4L$ , whereas  $\langle \ell_f \rangle$  in both the dimensions are much larger than this limit. Furthermore, linear dependence of  $\langle \ell_f \rangle$  on  $L$ , does not call for reanalysis of data via finite-size scaling method by replacing  $L$  by  $\langle \ell_f \rangle$ . Note that in Figs. 14 (c) and 14 (d) we presented results only up to  $L = 300$  and 100, respectively, by considering the fact that achieving freezing for very large systems is computationally very difficult, particularly when our observation suggests a linear relationship.

#### 4. Conclusion

We have studied pattern, growth and aging properties of the nearest neighbor ferromagnetic Ising model via Monte Carlo simulations [27], using Glauber spin-flip [27, 28] moves. Flips which did not change energy were accepted with two probabilities, viz.  $p = 1$  and  $1/2$ , referred to as the Metropolis and Glauber algorithms, respectively, to check for their relative effects on the behavior of various quantities. Our focus was on zero temperature quench, for both  $d = 2$  and 3. Quantitative information on the decay of the two time autocorrelation function was obtained via finite-size scaling [12, 13] and other methods of analysis. These were discussed with reference to the corresponding results for quenches to nonzero temperatures [12].

The autocorrelations exhibit nice scaling with respect to  $x (= \ell/\ell_w)$ . The late

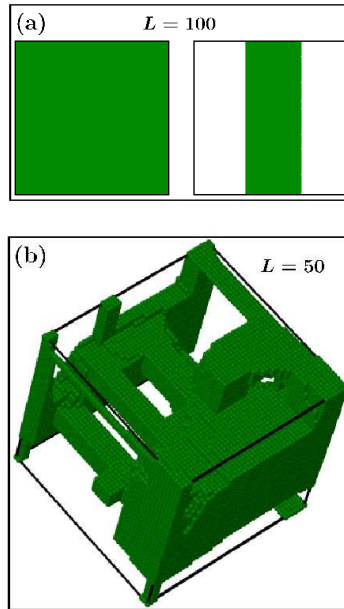


**Figure 13.** Typical final snapshots from representative configurations in (a)  $d = 2$  and (b)  $b = 3$ . These snapshots were obtained by using  $p = 1/2$ .

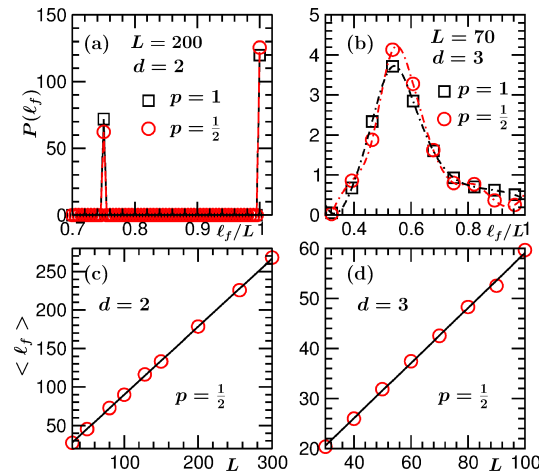


**Figure 14.** Plots of the distribution of final length,  $\ell_f$ , versus the scaled length  $\ell_f/L$ , for (a)  $d = 2$ ,  $L = 200$ ; (b)  $d = 3$  and  $L = 70$ . Average value of the final length is plotted versus system size, for  $p = 1/2$  in (c)  $d = 2$  and (d)  $d = 3$ . The solid lines represent linear fits to the simulation data sets.

time behavior is described by power-laws,  $C_{\text{ag}}(t, t_w) \sim x^{-\lambda}$ . At early time there exists correction that can be reasonably well described by an exponential factor. These features are very much similar to those for high temperature quenches [12].

In  $d = 2$ , the value of  $\lambda$  is in agreement with the LM value. However, the  $d = 3$  result differs significantly from the high temperature result [12], the latter being consistent with the LM value. The estimated value in this dimension not only differs from the LM prediction, but also appears to be far below the lower-bound of FH. We argue, via

analysis of the structure factor, in line with the derivation of YRD, that this is not a true violation if the small  $k$  behavior of  $S(k, t)$  is appropriately accounted for. Here note that the zero temperature structure in  $d = 3$  is incompatible with the well known Ohta-Jasnow-Kawasaki form.

As expected, all results are found to be nearly independent of aforementioned flipping probabilities. This is also true for the freezing property. For the latter we have demonstrated that the corresponding average length scale varies linearly with the system size. Close to the frozen length, the dynamics is very slow for  $d = 3$ . If an analysis is performed, to arrive at the domain growth law, via scaling of the corresponding relaxation time with the system size, a different, misleading conclusion can be arrived at. Recall that, from simulations of very large systems we confirmed that in this dimension also the growth at zero temperature follows the Lifshitz-Allen-Cahn law. We will address this issue of very late time dynamics in a future communication. Before closing, we mention that despite no dependence of growth exponent on the acceptance probability  $p$ , the growth in the  $p = 1/2$  case is slower than when  $p$  is set to unity, due to higher amplitude in the latter case. This fact is true, as expected, in both the space dimensions. Our observation suggests that finite-size effects also appear at a slightly smaller characteristic length scale for  $p = 1/2$ .

- [1] Bray A J 2002 *Adv. Phys.* **51** 481
- [2] Puri S and Wadhawan V (eds) 2009 *Kinetics of Phase Transitions* (CRC Press, Boca Raton)
- [3] Fisher D S and Huse D A 1988 *Phys. Rev. B* **38** 373
- [4] Liu F and Mazenko G F 1991 *Phys. Rev. B* **44** 9185
- [5] Majumdar S N and Huse D A 1995 *Phys. Rev. E* **52** 270
- [6] Yeung C, Rao M and Desai R C 1996 *Phys. Rev. E* **53** 3073
- [7] Corberi F, Lippiello E and Zannetti M 2006 *Phys. Rev. E* **74** 041106
- [8] Henkel M, Picone A and Pleimling M 2004 *Europhys. Lett.* **68** 191
- [9] Ohta T, Jasnow D and Kawasaki K 1982 *Phys. Rev. Lett.* **49** 1223
- [10] Arenzon J J, Cugliandolo L F and Picco M 2005 *Phys. Rev. E* **71** 032142
- [11] Lorenz E and Janke W 2007 *Europhys. Lett.* **77** 10003
- [12] Midya J, Majumder S and Das S K 2014 *J. Phys. : Condens. Matter* **26** 452202
- [13] Midya J, Majumder S and Das S K 2015 *Phys. Rev. E* **92** 022124
- [14] Allen S M and Cahn J W 1979 *Acta Metall.* **27** 1085
- [15] Yeung C 1988 *Phys. Rev. Lett.* **61** 1135
- [16] Majumdar S N, Huse D A and Lubachevsky B D 1994 *Phys. Rev. Lett.* **73** 182
- [17] Das S K and Chakraborty S 2017 *Eur. Phys. J. Spec. Top.* **226** 765
- [18] Amar J G and Family F 1989 *Bull. Am. Phys. Soc.* **34** 491
- [19] Shore J D, Holzer M and Sethna J P 1992 *Phys. Rev. B* **46** 11376
- [20] Lipowski A 1999 *Physica A* **268** 6
- [21] Cueille S and Sire C 1997 *J. Phys. A* **30** L791
- [22] Corberi F, Lippiello E and Zannetti M 2008 *Phys. Rev. E* **78** 011109
- [23] Olejarz J, Krapivsky P L and Redner S 2011 *Phys. Rev. E* **83** 051104
- [24] Olejarz J, Krapivsky P L and Redner S 2011 *Phys. Rev. E* **83** 030104
- [25] Chakraborty S and Das S K 2016 *Phys. Rev. E* **93** 032139
- [26] Chakraborty S and Das S K 2017 *Europhys. Lett.* **119** 50005
- [27] Landau D P and Binder K 2009 *A Guide to Monte Carlo Simulations in Statistical Physics*, (Cambridge University Press, Cambridge)
- [28] Glauber R J 1963 *J. Math. Phys.* **4** 294

- [29] Fisher M E 1971 *Critical Phenomena* ed M S Green (Academic, London)
- [30] Fisher M E and Barber M N 1972 *Phys. Rev. Lett.* **28** 1516
- [31] Heermann D W, Yixue L and Binder K 1996 *Physica A* **230** 132
- [32] Das S K 2015 *Molecular Simulation* **41** 382
- [33] Van Beijern H and Nolden I 1987 in *Structure and Dynamics of Surfaces II: Phenomena, Models and Methods, Topics in Current Physics, vol. 43* ed W Schommers and P Von Blanckenhagen (Berlin, Springer)
- [34] Spirin V, Krapivsky P L and Redner S 2001 *Phys. Rev. E* **63** 036118
- [35] Mullick P and Sen P 2017 *Phys. Rev. E* **95** 052150
- [36] Majumder S and Das S K 2010 *Phys. Rev. E* **81** 050102
- [37] Huse D A 1986 *Phys. Rev. B* **34** 7845.
- [38] Majumder S and Janke W 2016 *Phys. Rev. E* **93** 032506
- [39] Fisher M E 1967 *Rep. Prog. Phys.* **30** 615
- [40] Porod G 1982 in *Small-Angle X-ray scattering* ed O Glatter and O Kratky (Academic Press, New York, 42)
- [41] Oono Y and Puri S *Mod. Phys. Lett. B* **2** 861
- [42] Das S K 2012 *Europhys. Lett.* **97** 46006
- [43] Das S K 2013 *Phys. Rev. E* **87** 012135
- [44] Mani E and Löwen H 2015 *Phys. Rev. E* **92** 032301
- [45] Tung C, Harder J, Valeriani C and Cacciuto A 2016 *Soft Matter* **12** 555
- [46] Olejarz J, Krapivsky P L and Redner S 2012 *Phys. Rev. Lett.* **109** 195702